Talanta 81 (2010) 1339–1345

Contents lists available at ScienceDirect

Talanta

journal homepage: www.elsevier.com/locate/talanta

Optical investigations on ATP-induced aggregation of positive-charged gold nanoparticles

Chun Mei Li[a], Yuan Fang Li[a], Jian Wang[a], Cheng Zhi Huang[a,b,*]

[a] Education Ministry Key Laboratory on Luminescence and Real-Time Analysis, College of Chemistry and Chemical Engineering, Southwest University, Chongqing 400715, China
[b] College of Pharmaceutical Sciences, Southwest University, Chongqing 400715, China

ARTICLE INFO

Article history:
Received 19 December 2009
Received in revised form 4 February 2010
Accepted 7 February 2010
Available online 13 February 2010

Keywords:
Gold nanoparticles
ATP
ATP analogs
Aggregation

ABSTRACT

With the aids of localized plasmon resonance absorption and light-scattering measurements in this contribution, we investigated the aggregation of cetyltrimethylammonium bromide (CTAB) capped gold nanoparticles (AuNPs) in the presence of adenosine triphosphate (ATP). It was found that gradual aggregation of AuNPs occurs under physiological conditions with increasing ATP concentration from 200.0 to 400.0 μM, but the aggregates get dispersed again with much more increase of ATP concentration than 800.0 μM, corresponding with the color change from red to blue and to red again. Mechanism investigations showed that the aggregation of the AuNPs is likely induced by two interaction modes. One is the electrostatic interaction between the phosphate anions associated with the ATP and AuNPs owing to the cationic surfactant on the surfaces of AuNPs, and the other is the interaction between gold atom and nitrogen-containing bases. Further investigations showed that this aggregation mechanism could extend to the interactions between positively charged AuNPs with other analogs of ATP, such as guanosine triphosphate (GTP) and cytidine triphosphate (CTP).

1. Introduction

Gold nanoparticles (AuNPs), owing to their intrinsic characteristics of biocompatibility, catalytic activity, long-term stability, high extinction coefficients and strongly distance-dependent optical properties, have received much attention and found wide applications [1–7]. For example, relying on the color changes owing to the variation of interparticle distances, which can result different plasmon resonance absorption (PRA), they have been widely used as colorimetric probes. Depending on the distance of interparticles, larger or smaller than their average diameter, AuNPs exist either in dispersed or aggregated states, both of which are visually red and purple [3,4,8–10]. Thus, following the color shift of dispersed and aggregated states of AuNPs, colorimetric sensors have been developed for DNA [11,12], metal ions [13–16], organic small molecules or drugs [6,15,17–19], and proteins [4,7,20–22]. Meanwhile, AuNPs could be used as optical materials owing to the changes of the PRA of AuNPs. Therefore, understanding on the aggregation mechanism of AuNPs is important and attractive. However, AuNPs in these reports are usually prepared by reducing $HAuCl_4$ with citrate sodium, and it is no doubt that they are capped with citrate group. The shortcoming of this preparation protocol is that the as-prepared AuNPs are normally unstable in high salt aqueous medium and aggregation easily occurs. That property greatly confines the broad use of AuNPs in biological assays since therein high content of salt in buffers are generally employed [23,24]. Therefore, efforts have been made in order to adjust the colloidal stability such as the modification of surface charges, which can keep the electrostatic stabilization through the loss (or screening) of surface charges [22,24–27]. In such cases, some surfactants, such as the cationic surfactant including cetyltrimethylammonium bromide (CTAB), have been utilized as surface stabilizers in the synthesis of nanoparticles [28,29]. Since the activity of the surface atoms of the colloidal particles gets greatly reduced, metal nanoparticles capped with CTAB usually have good stability and are well dispersed [27], wherein CTAB molecules are adsorbed on the surface of the metal nanoparticles and form a bilayer structure, in which the inner layer is bound to the metal surface *via* the headgroups and the outer layers are connected through hydrophobic interactions [25–28].

It is known that ATP and ATP analogs are important substrates in living organisms. For example, as a major energy currency of the living cell, ATP plays an important role in regulating cellular metabolism and biochemical pathways in cell physiology [30]. Besides, the ATP level on a surface or in a medium of a living cell is a useful indicator of biological contamination that origins from

* Corresponding author at: Education Ministry Key Laboratory on Luminescence and Real-Time Analysis, College of Chemistry and Chemical Engineering, Southwest University, No. 2, Tiansheng Road, Beibei, Chongqing 400715, China.
Tel.: +86 23 68254659; fax: +86 23 68866796.
E-mail address: chengzhi@swu.edu.cn (C.Z. Huang).

0039-9140/$ – see front matter © 2010 Elsevier B.V. All rights reserved.
doi:10.1016/j.talanta.2010.02.032

human or bacterial [31]. Therefore, ATP detection is very important for studying cellular events such as proliferation and apoptosis, as well as hygiene monitoring in industry [18]. On the other hand, AuNPs have been used as cellular imaging materials based on their intrinsic characteristics, and their further application in biological processes is desirable. To the best of our knowledge, little information is known about the effects of ATP on the stability and aggregation potential of nanomaterials. Hence, understanding the stability and aggregation potential of AuNPs in the presence of ATP is critical for their further use in optical materials and biological applications.

2. Experimental

2.1. Materials

Adenosine triphosphate (ATP), adenosine diphosphate (ADP), adenosine monophosphate (AMP), guanosine triphosphate (GTP), cytidine triphosphate (CTP), and uridine triphosphate (UTP) were obtained from Sigma (St. Louis, MO). Sodium borohydride ($NaBH_4$) was obtained from Huanwei Fine Chemical Co., Ltd. (Tianjin, China). L-Ascorbic acid (L-AA) and sodium tripolyphosphate (PPPi), sodium pyrophosphate (PPi), and Na_3PO_4 were obtained from Chuandong Chemical Group Co., Ltd. (Chongqing, China). Cetyltrimethylammonium bromide (CTAB) and hydrogen tetrachloroaurate(III) tetrahydrate ($HAuCl_4{\cdot}4H_2O$) were purchased from Sinopharm Group Chemical regent Co., Ltd. (Shanghai, China).

Stock solutions were prepared with 2.0×10^{-3} mol L^{-1} $HAuCl_4{\cdot}4H_2O$, 0.01 mol L^{-1} $NaBH_4$, 0.10 mol L^{-1} L-ascorbic acid (L-AA), 0.20 mol L^{-1} CTAB. Tris–HCl buffer solution (pH 7.4) was employed to adjust the acidity of the aqueous solutions. All chemicals were analytical reagents and were used without further purification. Milli-Q purified water (18.2 MΩ) was used for all sample preparations.

2.2. Apparatus

UV–vis spectra were recorded with a Hitachi U-3010 spectrophotometer (Hitachi, Tokyo, Japan). The scanning electron microscope (SEM) images of AuNPs were performed with a Hitachi S-4800 scanning electron microscope (Tokyo, Japan) operating at 30.0 kV, and dark-field light-scattering images were caught with an Olympus E-510 camera (Tokyo, Japan) that was mounted on an Olympus BX 51 System Microscope (Tokyo, Japan). Solution-based ζ-potential and light-scattering analyses were completed on a Zetasizer Nano-ZS90 System (Malvern Inc.). FT-IR spectra were obtained by a Bruker Tensor 27 spectrophotometer (Germany) in KBr wafer. Photographs were taken with Olympus E-510 digital camera (Tokyo, Japan). A vortex mixer QL-901 (Haimen, China) was employed to mix the solutions.

2.3. Preparation of CTAB-capped AuNPs

CTAB-capped AuNPs were prepared by seed-mediated method with two-step procedures [23,32]. Firstly, a 5.0 mL solution of gold seeds was prepared by reducing $HAuCl_4{\cdot}4H_2O$ (2.5×10^{-4} mol L^{-1}) with ice-cold $NaBH_4$ (6.0×10^{-3} mol L^{-1}) in the presence of CTAB (7.5×10^{-2} mol L^{-1}). $NaBH_4$ solution should be freshly prepared and added at once to the solution. After being mixed vigorously for about 30 s, the mixture became light brown rapidly and could be used as seeds for further synthesis of AuNPs after 2–24 h aging at 25 °C.

10.0 mL 0.2 mol L^{-1} CTAB was then added to the growth solution, which contains 1.03 mL of 2.4×10^{-2} mol L^{-1} $HAuCl_4{\cdot}4H_2O$ and 5.22 mL H_2O. The color of the mixture quickly changed from light yellow to orange. Followed by the addition of 7.5 mL 0.10 mol L^{-1} freshly prepared L-AA, the mixture was gently mixed by inversion for about 2 min, during which the color of the solution immediately became colorless. Then, 62.5 μL of above 2 h-aged Au seeds solution was put into the growth solution and blended vigorously for 20 s, with the appearance of red color gradually. At last, the mixed solution was left undisturbed for 24 h at 25 °C. The prepared AuNPs are about 25 nm in diameter and positively charged as a result of the adsorption of the cationic surfactant (CTAB) on the surface of AuNPs. In this contribution, the concentration of gold was expressed as the concentration of Au atom in $HAuCl_4{\cdot}4H_2O$.

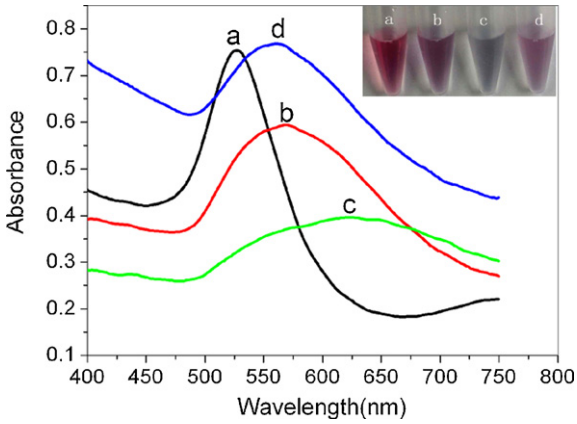

Fig. 1. UV–vis absorption spectra and color changes of AuNPs (0.2 mM) in the absence and presence of different concentrations of ATP. ATP concentrations: (a) 0, (b) 200.0, (c) 400.0, and (d) 800.0 μM. The photographs and the spectra were recorded after 10 min. Tris–HCl solution (10 mM, pH 7.4).

2.4. Aggregation investigations

Mixtures (500 μL) of CTAB-capped AuNPs (0.2 mM) and Tris–HCl (10 mM, pH 7.4) solutions were placed in a 1.5 mL plastic vial, with the presence of different concentrations of ATP. After vortex, the mixtures were maintained at room temperature for 10 min and then their absorption spectra were measured by a Hitachi U-3010 spectrophotometer (Hitachi, Tokyo, Japan).

The samples for SEM were first centrifuged at 12,000 r/min for 10 min at 25 °C to remove the excess CTAB, and then the precipitate was redispersed in distilled water and 3 μL of the solution was dropped onto the silica slice, followed by drying at room temperature.

The samples for dark-field imaging were also first centrifuged at 12,000 r/min for 10 min at 25 °C to remove the excess CTAB, and then the precipitate was redispersed in distilled water and 2 μL of the solution was dropped onto the glass slide.

3. Results and discussion

3.1. ATP-induced aggregation of AuNPs

To determine the effect of ATP on the aggregation of CTAB-capped AuNPs, we measured the optical properties of AuNPs at first. Fig. 1 shows the UV–vis absorption spectra of AuNPs (0.2 mM) and the color changes of the solutions in the absence and presence of different amounts of ATP, respectively. The PRA wavelength and band width are determined in part, which could indicate the particle size distribution of the aggregated AuNPs. The dispersed AuNPs are red (Fig. 1a) and their surface PRA is characterized at 524 nm (Fig. 1, curve a) (for interpretation of the references to color in this sentence, the reader is referred to the web version of the article). With increasing ATP concentrations, the solution then gets purple and the wavelength shifts to 600 nm, indicating that the

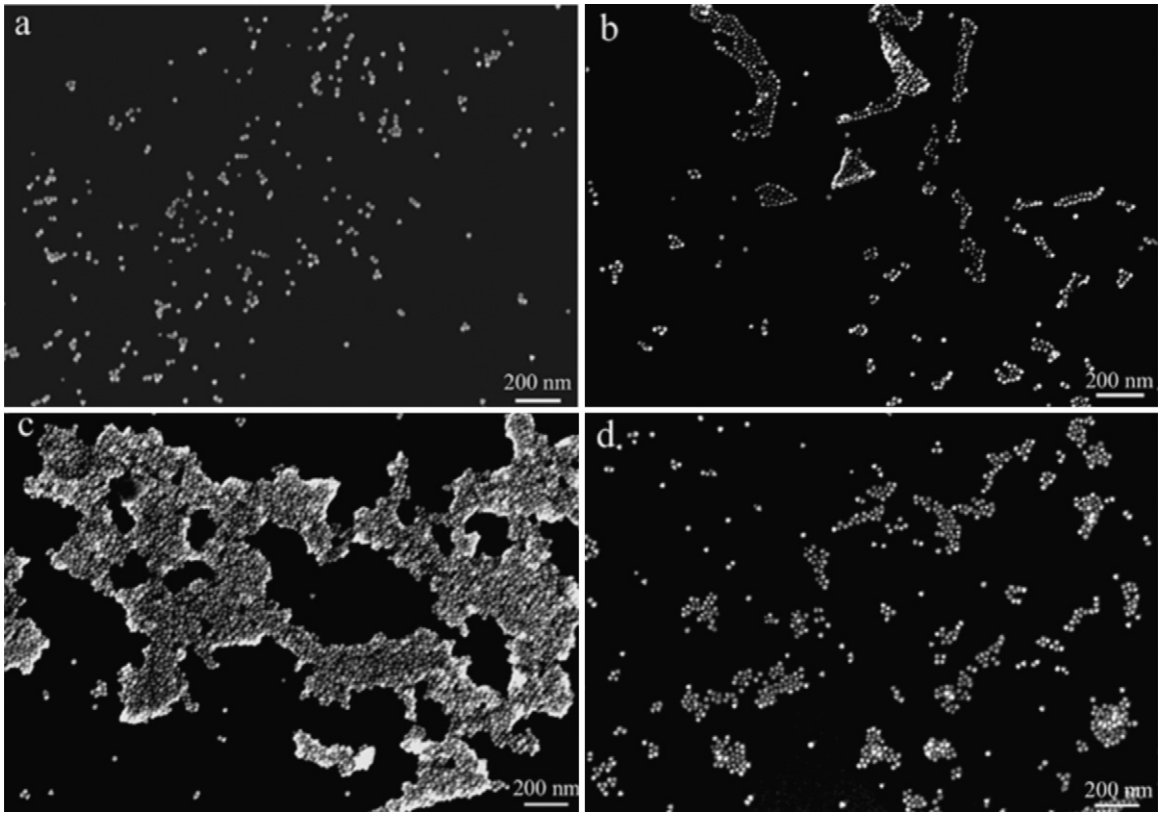

Fig. 2. The SEM images of AuNPs (0.2 mM) in the presence of different concentrations of ATP. ATP concentrations: (a) 0, (b) 200.0, (c) 400.0, and (d) 800.0 μM. Tris–HCl solution (10 mM, pH 7.4).

aggregation of AuNPs has occurred. Considering the ratios of the absorbance at 600 and 524 nm (*A*600/*A*524) are related to the quantities of dispersed and aggregated AuNPs, respectively, we define the *A*600/*A*524 ratio to express the aggregation degree of AuNPs [4,13,33].

It is obvious that the aggregation degree of AuNPs is greatly affected by ATP concentrations. Initially, the surface PRA wavelength at 524 nm experiences a red shift to approximately 568 nm when ATP concentration is below 200.0 μM, with a significant half-width broadened from 63 to 114 nm and a decrease of the absorbance at 524 nm (Fig. 1, curve b), indicating that the aggregation of AuNPs has begun. As the particles aggregate, the size range of aggregated structures grows broader because of the kinetics of the aggregation. With continuously increasing ATP concentration to 400.0 μM, the color changed from purple to blue distinctly (Fig. 1c), and concomitantly the PRA band gets much more broad with a half-width of 191 nm (Fig. 1, curve c), indicating that significant aggregation of the AuNPs occurred. Since the observed band is simply the sum of the absorbances of the individual particles, as the particles grow, the observed wavelength shifts to the red. And because the particle size distribution widens, so does the bandwidth. With further increasing ATP concentration to 800.0 μM, the PRA band shifts back to 560 nm (Fig. 1, curve d) with a half-width of 103 nm, indicating that some aggregates species might have been dissolved.

With increasing ATP concentrations, the surface PRA wavelength of AuNPs undergoes a red shift and then a blue shift, reflecting that the size of AuNPs aggregates changes with a concomitant change in PRA wavelength. Probably, the electron density of AuNPs and the refractive index of the surrounding medium are also changed concomitantly. This result provides a promising approach for modulating the state of dispersed/aggregated nanoparticles with tunable PRA features over a visible region of 450–750 nm.

3.2. Characterization of AuNPs aggregation in the presence of ATP

In order to further estimate the aggregation process of AuNPs, we used a set of analytical characterization methods to confirm the aggregation of the AuNPs, including scanning electron microscopy (SEM), dark-field light scattering (DFLS) images, ζ-potential and dynamic light scattering (DLS) analyses. DFLS image is a useful tool to observe the changes in the particle stability and aggregation by their different scattering images [6,34]. Figs. 2 and 3 displayed SEM and DFLS images of the AuNPs in the absence and presence of different concentrations of ATP, respectively. Owing to the weak light scattering and faster diffusion of the single AuNPs [6], it was hard to observe the scattering light from dispersed AuNPs by our DFLS system (Fig. 3a). In the presence of 200.0 μM ATP, however, the images in Fig. 2(b) showed mild aggregation of AuNPs and correspondingly a spot of scattering light was observed in Fig. 3(b). Comparatively, when the ATP concentrations get increased to 400.0 μM, intense aggregation of the AuNPs occurred as shown in Fig. 2(c), and strong scattering observed as Fig. 3(c) shown. The orange and red spots correspond to scattering images of AuNPs aggregate. With further increasing the ATP concentration, the degree of AuNPs aggregation decreased (Fig. 2(d) and Fig. 3(d)). They all provide strong evidence for the different aggregation state of the AuNPs under different concentrations of ATP in the Tris buffer (10 mM, pH 7.4).

From the SEM images, it is evident that AuNPs spontaneously assemble into chainlike assemblies. It is presented that no any separate nanoparticle could be found on the microgrid, which reveals that AuNPs prefer linear aggregate formation [35]. So it is desirable that we found a very simple approach to get nanoscale

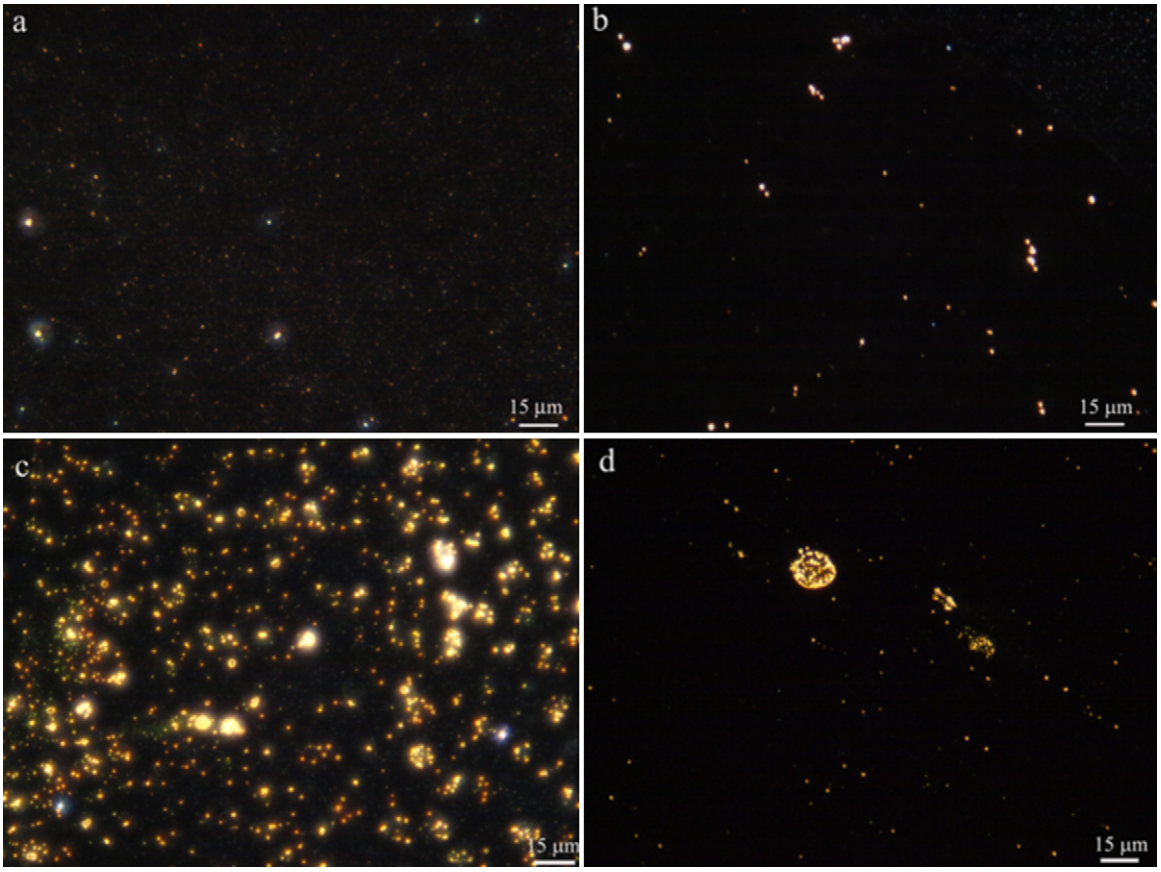

Fig. 3. The dark-field light-scattering images of AuNPs (0.2 mM) in the presence of different concentrations of ATP. ATP concentrations: (a) 0, (b) 200.0, (c) 400.0, and (d) 800.0 μM. Tris–HCl solution (10 mM, pH 7.4).

chainlike gold aggregates by linking individual CTAB-capped AuNPs with ATP molecules. That is, ATP molecule may be used to assemble nanoparticles advantageously by "soft–soft" interaction of nitrogen-containing bases functional groups adsorbed on the surfaces of nanoparticles [35].

Comparatively, DLS analyses and ζ-potential were extremely powerful tools to confirm the aggregation state of the AuNPs in the reaction solution. The result is presented in Fig. 4. When the AuNPs synthesized was dissolved in water, an average hydrodynamic diameter of 33.6 nm was obtained. When the AuNPs were dissolved in a low concentration of ATP (e.g., 100.0 μM), little aggregation was evident from the obtained particle size of 37.6 nm. When the ATP concentration increased to 200.0 μM, a slight aggregate size

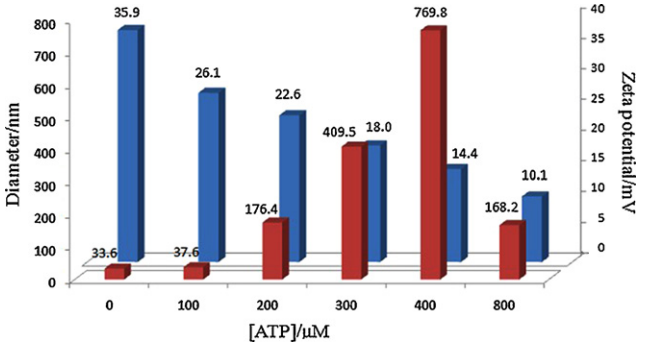

Fig. 4. DLS aggregate size (camine columns) and ζ-potential (blue columns) comparisons for AuNPs (0.2 mM) in the presence of different concentrations of ATP. Tris–HCl solution (10 mM, pH 7.4). (For interpretation of the references to color in this figure legend, the reader is referred to the web version of the article.)

of 176.4 nm was obtained. Then a larger aggregate size of 769.8 nm was observed when increase the ATP concentration to 400.0 μM. The increased aggregate sizes suggest the great degree of destabilization of AuNPs. Smaller aggregate with the size of 168.2 nm is further observed at ATP concentrations of 800.0 μM.

In addition, the ζ-potential analysis of the aggregates presented in Fig. 4 was consistent with the average diameter result. It is shown that a trend of decreasing surface potentials of AuNPs is determined with increasing ATP concentration. Initially, the as-prepared AuNPs possessed a ζ-potential of 35.9 mV. Then it decreased to 22.6 mV when AuNPs were dissolved in 200.0 μM ATP. This number gradually decreased to 14.4 mV as ATP concentration increased to 400.0 μM. If it is higher than 800.0 μM, a smaller ζ-potential was available, only 10.1 mV. It is obvious that the particles gradually destabilize when dissolving with large concentrated ATP molecules. The trend in ζ-potential demonstrates a minimization of the surface charge states, from highly positive to nearly neutral, indicating that the AuNPs surface that capped with positively charged CTAB molecule is likely to electrostatically bind the trivalent anions in ATP molecule in solution.

3.3. Mechanism investigations on ATP-induced aggregation of AuNPs

Based upon the observed trends of PRA band shifting, SEM images demonstrating aggregation, changes in the ζ-potential, and the DLS-based size/assembly analysis, we conclude that the aggregation of AuNPs can be induced by different concentrations of ATP under physiological conditions. Fig. 5 displays the plasmon maximum λ_{max} and the *A*600/*A*524 ratio as a function of ATP concentration, respectively. From Fig. 5 (left), it is evident that the shift

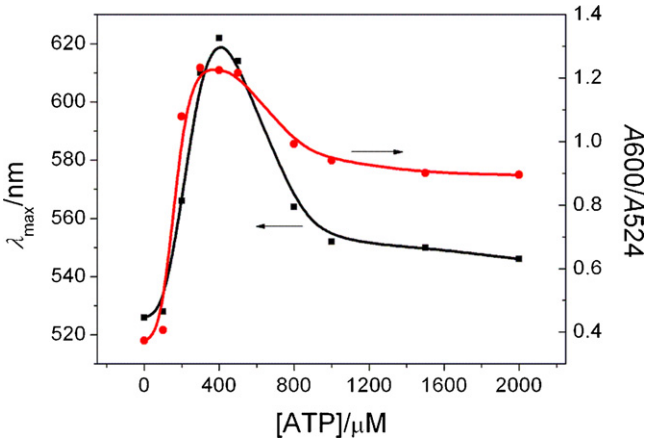

Fig. 5. The plasmon maximum λ_{max} (left) and the *A*600/*A*524 ratio (right) as a function of ATP concentration. Tris–HCl solution (10 mM, pH 7.4).

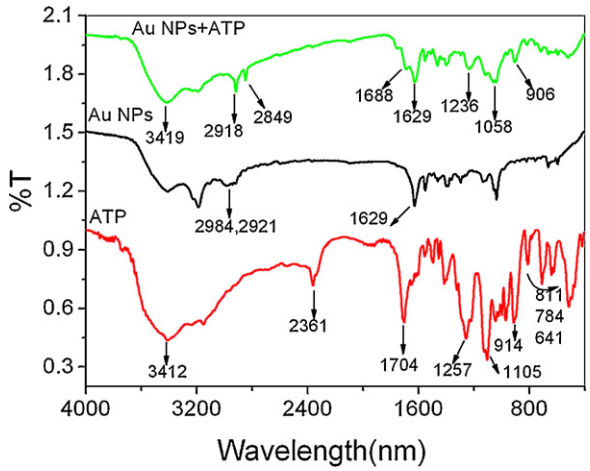

Fig. 6. The IR spectra of AuNPs, ATP and the adduct of AuNPs and ATP after 10 min.

of the absorption spectra peak for AuNPs depends strongly upon the concentration of ATP. The peak position appears a red shift as the ATP concentration gradually increases to 400.0 μM, then it turns to a blue shift with the increased ATP concentration. The aggregation reached maximum values at 400.0 μM of ATP. Fig. 5(right) showed that there was a linear relationship between the *A*600/*A*524 ratios and the ATP concentration (<400.0 μM). So we point out that the quantitative determination of ATP concentration (<400.0 μM) based on the aggregation of the AuNPs can be achieved. It is important to note that the Tris buffer (10 mM, pH 7.4) has little effect on the AuNPs stability (date not shown) [29].

We have also monitored the shift in the surface PRA of AuNPs as a function of time to investigate the kinetics of the aggregation process (Supporting Information, Fig. S1). It showed that the aggregation of AuNPs induced by ATP required only about 10 min to completion. This is likely the result of electrostatic aggregation of the AuNPs through the templating of ATP anions along the cationic AuNPs surface, thus minimizing electrostatic repulsion and leading to aggregation. This phenomenon is consistent with the non-crosslinking aggregation mechanism.

The stability of AuNPs in solution is dictated by two key factors: electrostatic repulsion between the charged AuNPs and steric constraints, both of which are attributable to the CTAB surfactant. The surfactant is positively charged under any condition due to the quaternary ammonium head group of the molecule. The anions including the negative charges in phosphate backbone of ATP molecules, as well as the hydroxide ions present at Tris buffer pH 7.4, can electrostatically bind to the cationic surface. Upon electrostatic binding of the anions to the AuNPs surface, the overall positive charge of the AuNPs decreases as determined by ζ-potential analysis, thus the electrostatic repulsion among the AuNPs is decreased. At this time, the AuNPs reach an interparticle distance and the London-van der Waals attractive forces dominate to result in rapid aggregation (see Scheme 1).

When ATP concentration is higher than 800.0 μM, the formation of aggregation gets decreased as a result of repulsion and steric effects because the surface of the AuNPs quickly became saturated with ATP molecules. Therefore, the ATP-saturated AuNPs are stable mainly as a result of Coulombic repulsion, similar as the reference mentioned [4].

Further experiment has been made using an FT-IR technique to verify the structure changes after the interaction between ATP and AuNPs. As shown in Fig. 6, the remarkable differences of ATP–AuNPs adduct were observed at IR bands 2361, 1704, 1257, 1105 and 914 cm^{-1}. Band at 1704 cm^{-1} assigned to the stretching vibrations of C=N was shifted to 1688 cm^{-1}, representing the surroundings of C=N changes (due to the interaction between gold and nitrogen atoms). Bands at 1257 and 1105 cm^{-1} assigned to the anti-symmetric and symmetric stretching modes of the P=O group in ATP molecule were shifted to 1236 and 1058 cm^{-1}, respectively. At the same time, the band at 914 cm^{-1} assigned to the

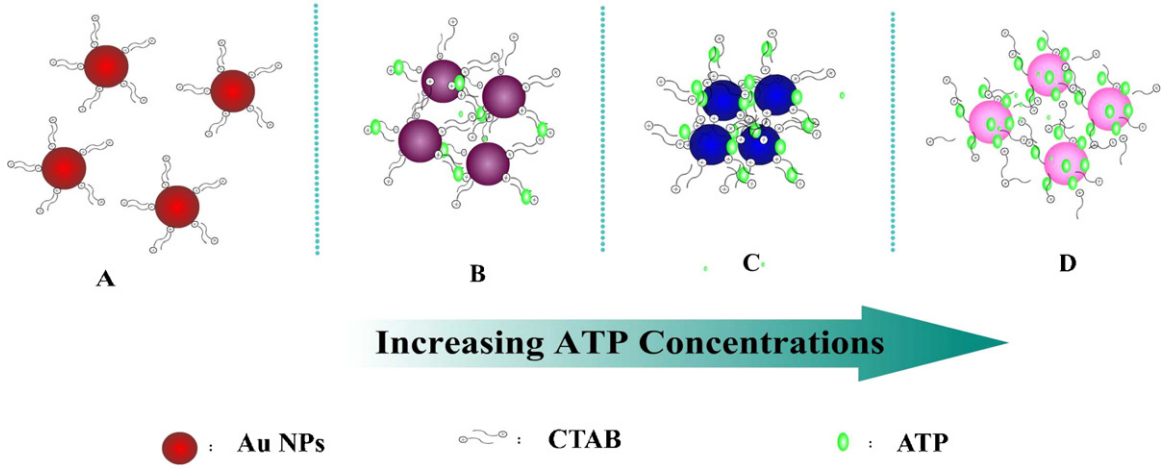

Scheme 1. Schematic representation of the control of CTAB-capped AuNPs (a) and the aggregation of CTAB-capped AuNPs in the presence of ATP at (b) low, (c) medium, and (d) high concentrations.

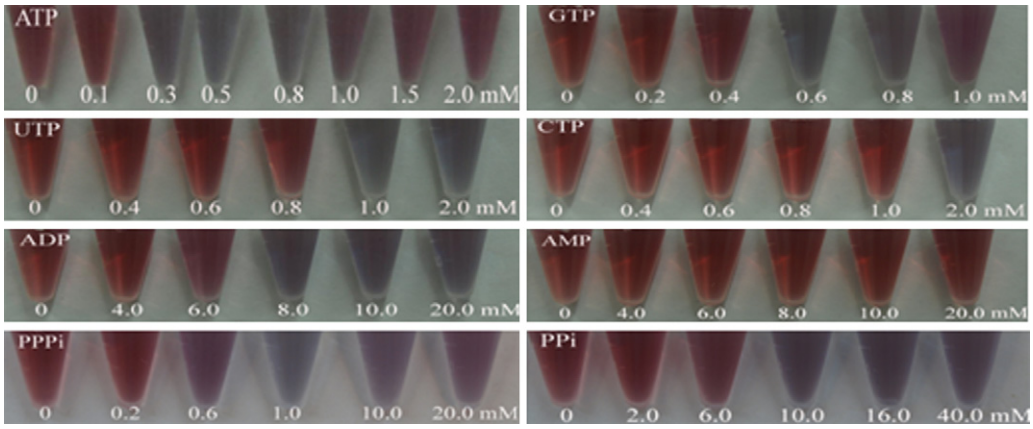

Fig. 7. Colors of AuNPs (0.4 mM) in the presence of different concentrations of ATP, GTP, UTP, CTP, ADP, AMP, PPPi, PPi. The photographs were taken immediately after the addition of ATP, GTP, UTP, CTP, ADP, AMP, PPPi, PPi, AuNPs in 10 mM Tris–HCl solution (pH 7.4).

stretching mode of P–O–P was shifted to 906 cm^{-1} in the adduct. These results indicated the formation of an adduct resulted in lower wave-number shift of P–O group due to the hydrogen bonding. Meanwhile the bands at 3412 cm^{-1} assigned to the anti-symmetric and symmetric stretching vibrations of N–H of the exocyclic amino group of ATP were shifted to 3419 cm^{-1} in the adduct. 2984 and 2912 cm^{-1} assigned to the anti-symmetric and symmetric stretching vibrations of CH_2 in straight-chain hydrocarbons of the CTAB capped on the AuNPs, which correspondingly shifted to 2918 and 2849 cm^{-1} in the adduct spectrum (details see Table S1 in Supporting Information).

So it can be believed that the nitrogen heterocyclic group of ATP has taken part in the interaction between ATP and AuNPs, and the conformations of AuNPs and ATP have been changed during the formation of the adduct. The results of IR spectra indicate that the recognition or interaction sites are the nitrogen heterocyclic group of ATP and γ-phosphate of ATP. As for the binding mode, it was presumed that γ-phosphate of ATP approached the quaternary ammonium head group of CTAB by electrostatic force, and the nitrogen heterocyclic group of ATP approached the Au atom (Au–N) [36–38]. When the distance is close enough to form a hydrogen bond, the two molecules can form a stable structure adduct by such a hydrogen bonding.

3.4. Aggregation of gold nanoparticles induced by ATP analogs

Since all of the nucleosides have functional groups (amines, carbonyls, etc.) that could act as ligands for the AuNPs surface as well as phosphate groups along the backbone that could electrostatically bind [39], we further experimented the effects of the ATP analogs (GTP, CTP, UTP, ADP, AMP, PPPi, and PPi) on CTAB-capped AuNPs aggregation and the result was shown in Fig. 7. We found these compounds have the similar phenomena in inducing AuNPs aggregation. There were distinctly different assembly behaviors of AuNPs in the presence of different concentrations of ATP analogs, respectively. So a simple method to distinguish these nucleotides using AuNPs as a colorimetric probe is set up. Since the minimal concentrations of these nucleotides to induce AuNPs aggregation are different, we concluded that the relative adsorption affinities of nucleotides to AuNPs are different, following the sequence ATP > GTP > PPPi > UTP > CTP > ADP > PPi > AMP. We further believe that the different affinities to AuNPs are mostly due to two factors: the different functional groups (amines and carbonyls) and the different negatively charged phosphate groups exist in the nucleotides, namely the more functional groups and negatively charged phosphate groups exist, the greater affinities to AuNPs are. In addition, as most of the nucleotides chemisorbed on gold atom through multiple binding sites, the different types of possible surface binding moieties (e.g., carbonyls and amides; mono-versus polydentate) may also affect the observed affinities, as mentioned in the references [36,37].

4. Conclusions

In this contribution, we have provided a promising approach to modulate the AuNPs with desirable stable/aggregated property using different concentrations of ATP from 200.0 to 800.0 μM. Correspondingly, the PRA band of AuNPs over a visible region of 450–750 nm was tunable by ATP. Based upon these excellent properties, AuNPs have been potentially broadened their applicability for constructing nanocomposite films with modulated optical property on various solid substrates or applying as ideal signal transducers for colorimetric assays.

On the other hand, we have reported a novel colorimetric assay to distinguish ATP analogs based on their discriminated effects on the aggregation of nanoparticles. This result provides the potential feasibility of high throughput assays in microwell-based plates or paper-based bioassays using AuNPs as colorimetric probes. Our future efforts could be focused on studying the structural characteristics of the oligonucleotide layers adsorb on the AuNPs and the secondary interaction between the nucleosides that comprise the oligonucleotide and the gold surface.

Acknowledgements

The authors herein express their great appreciation for the financial support by the National Natural Science Foundation of China (No. 90813019) and the Chongqing Science and Technology Commission for the Chongqing Key Laboratory on Luminescence and Real-Time Analysis (2006CA8006).

Appendix A. Supplementary data

Supplementary data associated with this article can be found, in the online version, at doi:10.1016/j.talanta.2010.02.032.

References

[1] H. Wei, C. Chen, B. Han, E. Wang, Anal. Chem. 80 (2008) 7051.
[2] M.-C. Daniel, D. Astruc, Chem. Rev. 104 (2004) 293.
[3] N.L. Rosi, C.A. Mirkin, Chem. Rev. 105 (2005) 1547.
[4] C.-C. Huang, Y.-F. Huang, Z. Cao, W. Tan, H.-T. Chang, Anal. Chem. 77 (2005) 5735.
[5] W. Wang, C. Chen, M. Qian, X.S. Zhao, Anal. Biochem. 373 (2008) 213.

[6] S.-J. Chen, Y.-F. Huang, C.-C. Huang, K.-H. Lee, Z.-H. Lin, H.-T. Chang, Biosens. Bioelectron. 23 (2008) 1749.
[7] Y. Wang, D. Li, W. Ren, Z. Liu, S. Dong, E. Wang, Chem. Commun. (2008) 2520.
[8] J.J. Storhoff, R. Elghanian, R.C. Mucic, C.A. Mirkin, R.L. Letsinger, J. Am. Chem. Soc. 120 (1998) 1959.
[9] X. He, H. Liu, Y. Li, S. Wang, Y. Li, N. Wang, J. Xiao, X. Xu, D. Zhu, Adv. Mater. 17 (2005) 2811.
[10] F. He, Y. Tang, S. Wang, Y. Li, D. Zhu, J. Am. Chem. Soc. 127 (2005) 12343.
[11] K. Sato, K. Hosokawa, M. Maeda, J. Am. Chem. Soc. 125 (2003) 8102.
[12] H. Li, L. Rothberg, Proc. Natl. Acad. Sci. U.S.A. 101 (2004) 14036.
[13] J. Liu, Y. Lu, J. Am. Chem. Soc. 125 (2003) 6642.
[14] L. Wang, X. Liu, X. Hu, S. Song, C. Fan, Chem. Commun. (2006) 3780.
[15] W. Zhao, W. Chiuman, J.C.F. Lam, S.A. McManus, W. Chen, Y. Cui, R. Pelton, M.A. Brook, Y. Li, J. Am. Chem. Soc. 130 (2008) 3610.
[16] C.-W. Liu, Y.-T. Hsieh, C.-C. Huang, Z.-H. Lina, H.-T. Chang, Chem. Commun. (2008) 2242.
[17] J. Liu, Y. Lu, Angew. Chem. Int. Ed. 45 (2006) 90.
[18] J. Wang, L. Wang, X. Liu, Z. Liang, S. Song, W. Li, G. Li, C. Fan, Adv. Mater. 19 (2007) 3943.
[19] W. Zhao, W. Chiuman, M.A. Brook, Y. Li, ChemBioChem 8 (2007) 727.
[20] V. Pavlov, Y. Xiao, B. Shlyahovsky, I. Willner, J. Am. Chem. Soc. 126 (2004) 117689.
[21] H. Wei, B. Li, J. Li, E. Wang, S. Dong, Chem. Commun. (2007) 3735.
[22] W. Zhao, W. Chiuman, J.C.F. Lam, M.A. Brook, Y. Li, Chem. Commun. (2007) 3729.
[23] J. Wang, Y.F. Li, C.Z. Huang, T. Wu, Anal. Chim. Acta 626 (2008) 37.
[24] W. Zhao, F. Gonzaga, Y. Li, M.A. Brook, Adv. Mater. 19 (2007) 1766.
[25] V. Patil, K.S. Mayya, S.D. Pradhan, M. Sastry, J. Am. Chem. Soc. 119 (1997) 9281.
[26] W. Cheng, S. Dong, E. Wang, Electrochem. Commun. 4 (2002) 412.
[27] A. Wu, W. Cheng, Z. Li, J. Jiang, E. Wang, Talanta 68 (2006) 693.
[28] B. Nikoobakht, M.A. El-Sayed, Langmuir 17 (2001) 6368.
[29] M. Sethi, G. Joung, M.R. Knecht, Langmuir 25 (2009) 317.
[30] J. Wang, Y. Jiang, C. Zhou, X. Fang, Anal. Chem. 77 (2005) 3542.
[31] J.A. Cruz-Aguado, Y. Chen, Z. Zhang, N.H. Elowe, M.A. Brook, J.D. Brennan, J. Am. Chem. Soc. 126 (2004) 6878.
[32] T.K. Sau, C.J. Murphy, J. Am. Chem. Soc. 126 (2004) 8648.
[33] J. Liu, Y. Lu, Anal. Chem. 76 (2004) 1627.
[34] J. Ling, Y.F. Li, C.Z. Huang, Anal. Chem. 81 (2009) 1707.
[35] S. Basu, S. Pande, S. Jana, S. Bolisetty, T. Pal, Langmuir 24 (2008) 5562.
[36] H. Kimura-Suda, D.Y. Petrovykh, M.J. Tarlov, L.J. Whitman, J. Am. Chem. Soc. 125 (2003) 9014.
[37] L.M. Demers, M. stblom, H. Zhang, N.-H. Jang, B. Liedberg, C.A. Mirkin, J. Am. Chem. Soc. 124 (2002) 11248.
[38] M. stblom, B. Liedberg, L.M. Demers, C.A. Mirkin, J. Phys. Chem. B 109 (2005) 15150.
[39] J.J. Storhoff, R. Elghanian, C.A. Mirkin, R.L. Letsinger, Langmuir 18 (2002) 6666.